RSC Advances

PAPER

Check for updates

Cite this: *RSC Adv.*, 2018, **8**, 33403

A novel Sm^{3+} singly doped $LiCa_3ZnV_3O_{12}$ phosphor: a potential luminescent material for multifunctional applications†

Heng Guo,[a] Balaji Devakumar,[a] R. Vijayakumar,[a] Peng Du*[b] and Xiaoyong Huang*[a]

Received 3rd September 2018
Accepted 21st September 2018

DOI: 10.1039/c8ra07329e

rsc.li/rsc-advances

The Sm^{3+} ion singly doped $LiCa_3ZnV_3O_{12}$ (LCZV) phosphors were synthesized by a traditional high-temperature solid-state method. The luminescence characteristics of the as-prepared samples were studied by photoluminescence excitation and emission spectra. Under 343 nm excitation, the synthesized phosphors exhibited color controllable emission induced by the efficient energy transfer from VO_4^{3-} groups to Sm^{3+} ions. Besides, the energy transfer efficiency was revealed to be about 58.4% when the dopant concentration was 4 mol%. By utilizing the as-prepared LCZV:Sm^{3+} phosphors, commercial $BaMgAl_{10}O_7:Eu^{2+}$ blue-emitting phosphors and a near-ultraviolet light-emitting diode (LED) chip, a white LED device was fabricated. Under an injection current of 100 mA, the packaged LED device emitted pure white light with high color rendering index (88.4) and proper correlated color temperature (4320 K). By analyzing the thermal quenching behavior of the VO_4^{3-} groups and Sm^{3+} ions, the optical thermometric behavior of the Sm^{3+}-doped LCZV compounds was investigated. The maximum absolute sensor sensitivity and relative sensor sensitivity were found to be 0.25 K^{-1} and 1.8% K^{-1}, respectively. Additionally, the emitting color of the studied samples was dependent on the temperature. Ultimately, the Sm^{3+}-doped LCZV phosphors were potential candidates for indoor illumination, optical thermometry and safety signals in high temperature environments.

1. Introduction

Recently, rare-earth ion doped inorganic phosphors have attracted much attention since they can be used in a variety of applications, such as solid-state lighting, displays, and solar cells.[1–8] As is well-known, vanadate compounds usually have a broad and intense charge transfer (CT) absorption band originating from the VO_4^{3-} groups. Moreover, when the vanadate compounds are excited by the CT band, these materials can exhibit a broad emission band in the visible region. Owing to these optical characteristics, the vanadate compounds are regarded as excellent luminescent materials. Furthermore, the VO_4^{3-} groups can transfer the captured energy to the dopants (usually rare-earth ions) through a nonradiative transition process, resulting in glaring emission in rare-earth ions doped vanadates.[9,10] The rare-earth ion doped vanadate-based phosphors have been widely studied due to their excellent optical properties and their abundant applications.[11–16] Among the rare-earth ions, Sm^{3+}, which has visible emissions in orange-red wavelength region arising from the $^4G_{5/2} \rightarrow {}^6H_{J/2}$ ($J = 7$, 9, and 11) transitions, has attracted much attention.[17,18] It was reported that the $NaGd_3(VO_4)_2:Sm^{3+}$ phosphors can emit the featured orange-red emissions of Sm^{3+} ions and had potential applications in solid-state lighting.[19] Nevertheless, as far as we know, there are no any reports to deal with the luminescence properties of Sm^{3+} ions doped $LiCa_3ZnV_3O_{12}$ (LCZV) phosphors. Therefore, to further comprehend the luminescent behaviors of the Sm^{3+} ions doped vanadates as well as their applications, it would be very necessary to synthesize the Sm^{3+}-doped LCZV phosphors and study their luminescence performance and their promising applications.

On the other hand, temperature is regarded as a crucial constant since it can induce some significant changes in the fields of industrial manufacture, medical diagnosis, scientific research, and daily life.[20–23] Hence, its monitoring with high spatial resolution and accuracy is important. Nowadays, the non-contact optical temperature sensor, which utilizes the fluorescence intensity ratio (FIR) route based on the temperature-dependent emission spectra of two thermally coupled levels of rare-earth ions, has been widely developed to measure the temperature of some inaccessible objects on account of its preponderances of high sensor sensitivity, fast response *et al.*[24,25] Through analyzing the energy level distribution of the rare-earth ions, some of them, such as Er^{3+}, Tm^{3+}, Nd^{3+} and Eu^{3+}, possess pairs of thermally coupled levels.[26,27]

[a]College of Physics and Optoelectronics, Taiyuan University of Technology, Taiyuan 030024, P. R. China. E-mail: huangxy04@126.com

[b]Department of Electronic Engineering, Kyung Hee University, Yongin-si, Gyeonggi-do 446-701, Republic of Korea. E-mail: dp2007good@sina.com

† Electronic supplementary information (ESI) available. See DOI: 10.1039/c8ra07329e

However, this strategy suffers from relatively small energy gap ($200 \leq \Delta E \leq 2000$ cm^{-1}) so as to allow the electrons can be exited from the low excited level to the high excited level by means of thermal activation. Consequently, the relative sensor sensitivity ($S_r = \Delta E/kT^2$) value of the rare-earth ion doped luminescent materials based on the aforementioned strategy is strictly limited because of the small energy gap.[28,29] Thus, some other strategies should be carried out to overcome this shortage. Currently, through utilizing the diverse responses of the dual emissions of rare-earth ions to the temperature, some admirable results have been achieved. Zhang *et al.*, revealed that the sensor sensitivity of the LaOBr:Ce^{3+}/Tb^{3+} phosphors reached up to 0.42% by studying the temperature-dependent FIR values between the Ce^{3+} and Tb^{3+} ions.[30] Furthermore, Chen *et al.* also demonstrated that the Er^{3+}/Cr^{3+}/Yb^{3+}-tridoped $LiGa_5O_8$ nanoparticles with sensor sensitivity of 0.35% were promising candidates for optical thermometry.[31] In spite of these achievements, more efforts are still required to enhance the optical thermometric performance of the rare-earth ions doped luminescent materials so as to make them are suitable for practical applications.

In present work, the conventional solid-state reaction method was employed to prepare the Sm^{3+}-doped LCZV phosphors. The phase compositions, morphology, energy transfer process and room-temperature luminescent properties of the resultant samples were studied. Furthermore, with help of the near-ultraviolet (NUV) light-emitting diode (LED) chip, commercial $BaMgAl_{10}O_7$:Eu^{2+} (BAM:Eu^{2+}) blue-emitting phosphors, and the as-synthesized LCZV:Sm^{3+} phosphors, a white-LED device was packaged to explore the feasibility of the Sm^{3+}-doped LCZV phosphors for solid-state lighting applications. Ultimately, the temperature sensing behaviors of the Sm^{3+}-doped LCZV compounds were also investigated through studying the diverse temperature responses of VO_4^{3-} groups and Sm^{3+} ions.

2. Experimental

Polycrystalline samples of $LiCa_{3(1-x)}ZnV_3O_{12}$:xSm^{3+} (LCZV:xSm^{3+}; $x = 0$, 0.002, 0.005, 0.01, 0.02, 0.03, and 0.04) phosphors were prepared by a conventional high-temperature solid-state reaction method. The stoichiometric amounts of Li_2CO_3 (analytical reagent; A.R.), $CaCO_3$ (A.R.), ZnO (A.R.), NH_4VO_3 (A.R.), and high-purity Sm_2O_3 (99.99%) were used as the raw materials. Then, the above chemicals were thoroughly mixed in an agate mortar. The obtained mixture was transferred into alumina crucibles, and pre-heated at 750 °C (5 °C min^{-1}) for 6 h under air atmosphere. After that, the products were reground and sintered again at 850 °C for 6 h in air. Finally, the as-synthesized samples were slowly cooled to room temperature in the furnace, and ground again into powders for future characterization.

The phase purity of the samples were identified by X-ray diffractometer (Bruker D8) using Cu Kα radiation ($\lambda = 1.54056$ Å) in the 2θ range from 10° to 80° with the scanning steps of 0.02. The morphology properties of the samples were obtained by a field-emission scanning electron microscope (FE-SEM; MAIA3 TESCAN). Diffuse reflectance spectra of samples were recorded by an UV-Vis-NIR spectrophotometer (SHIMADZU UV-2600) with $BaSO_4$ white plate used as a standard reference. The photoluminescence (PL) emission and PL excitation (PLE) spectra were recorded by the Edinburgh instruments FS5 spectrometer equipped with a 150 W continued-wavelength xenon lamp as the excitation source. The internal quantum efficiency (IQE) of the phosphor was measured using Edinburgh FS5 spectrometer equipped with an integrating sphere coated with barium sulphate. This system employs the PL method for measuring the IQE, which is defined as the ratio of the number of photons emitted to the number of photons absorbed by the material. The IQE value was calculated by quantum yield measurement software. All the measurements were performed at room temperature.

The commercial blue phosphors BAM:Eu^{2+} and as-prepared LCZV:0.01Sm^{3+} phosphors were mixed with silicone thoroughly, and the obtained phosphor/silicone mixture was coated on the surface of the LED chip to fabricate white LED device. The photoelectric properties of the fabricated LED device were measured by using an integrating sphere spectroradiometer system (HAAS-2000, Everfine). The LED was worked with 100 mA driven current. The spectral power distributions of LED device were measured using a corrected spectrometer to calculate their values of correlated color temperature (CCT) and color rendering index (CRI).

3. Results and discussion

3.1 Phase structure

The X-ray diffraction (XRD) pattern was applied to identify the phase compositions of the final products. The typical XRD patterns of the as-synthesized LCZV:xSm^{3+} phosphors with the doping concentration of 0, 0.2, 1, and 4 mol% were depicted in Fig. S1.† Since the cubic crystal structure of $LiCa_3ZnV_3O_{12}$ is isostructural with that of the $LiCa_3MgV_3O_{12}$, the Joint Committee on Powder Diffraction Standards (JCPDS) card no. 24-1212 was used as reference.[32,33] As presented, when the dopant content was small ($x \leq 0.01$), it can be seen that the entire detected profiles were the same and the diffraction peaks matched well with the standard JCPDS card, demonstrating that the obtained compounds had pure cubic phase. However, when the Sm^{3+} ion concentration was elevated to 4 mol%, several impure diffraction peaks, which were classified to the $SmVO_4$ (JCPDS#17-0876), were detected at 18.46°, 24.48°, and 33.01° apart from the phase of the LCZV.[34] The results showed that there was a solubility limitation for the Sm^{3+} ions in the LCZV host lattices.

In order to know the detailed crystal structure of the studied samples, the Rietveld XRD refinement was performed. As is known, to carry out the Rietveld XRD refinement, an initial crystal structure model, which contains a reasonable approximation of the actual crystal structure, is required.[17] In our work, the $LiCa_3MgV_3O_{12}$ was employed as the initial structural model because of its isostructural nature with the LCZV. Fig. 1(a) shows the observed (crosses), calculated (red lines) and difference (blue lines) XRD patterns of the LCZV:0.01Sm^{3+} phosphors. It can be seen that the calculated and observed XRD

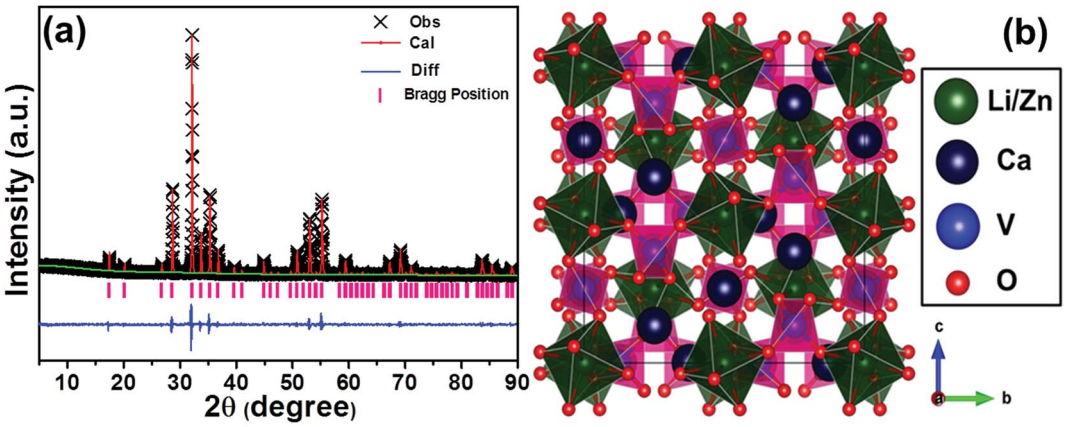

Fig. 1 (a) Observed (crosses) and calculated (red solid line) powder XRD pattern of the LCZV:0.01Sm^{3+} sample. The blue solid lines represent the difference between experimental and calculated data and the pink sticks mark the Bragg reflection positions. (b) Crystal structure of LCZV sample.

patterns coincided well with each other, implying that the LCZV:0.01Sm^{3+} phosphors possessed single cubic phase with $Ia\bar{3}d$ space group. Moreover, the reliability factors of the refinement were revealed to be $R_{wp} = 4.53\%$, $R_p = 6.26\%$, and $\chi^2 = 2.13$ (see Table S1†), indicating that the simulation results were reasonable. Furthermore, the cell constants of the LCZV:0.01Sm^{3+} compounds were calculated to be $a = b = c = 12.4437(1)$ Å and $V = 1926.86(3)$ $Å^3$ (see Table S1†). From the crystal unit cell structure (Fig. 1(b)), one knows that the LCZV host had a garnet structural. Specially, the Ca^{2+} ions located at eightfold dodecahedral sites and formed the [CaO_8] dodecahedra. The Zn^{2+} and Li^+ ions are both located in the same sites perch at 16a positions on the basis of the close ionic radii of Zn^{2+} ($r = 0.74$ Å, CN = 6) and Li^+ ($r = 0.76$ Å, CN = 6). The sites of V^{5+} ions with a 24d position form [VO_4] tetrahedral units. Due to their similar ionic radii, Sm^{3+} ($r = 1.079$ Å, CN = 8; $r = 0.958$ Å, CN = 6) could be expected to occupy Ca^{2+} ($r = 1.06$ Å, CN = 8) sites to form [SmO_8] dodecahedrons. Zn^{2+} ($r = 0.74$ Å, CN = 6) and Li^+ ($r = 0.76$ Å, CN = 6) sites are too small for them to enter in. (see Fig. 1(b) and Table S2†).[35]

The surface morphology behaviors of the as-prepared compounds were analyzed by utilizing the FE-SEM image. The representative FE-SEM images of LCZV:0.01Sm^{3+} sample with different magnifications are shown in Fig. 2(a) and (b). As presented in Fig. 2(a), it was evident that the as-synthesized compounds consisted of non-uniform microparticles. Furthermore, it can be seen from the high-magnification FE-SEM image (Fig. 2(b)) that the particle size ranged from approximately 2 to 6 μm.

3.2 Photoluminescence properties

Fig. 3(a) depicts the diffuse reflectance spectra the of LCZV and LCZV:0.01Sm^{3+} phosphors in the 200–800 nm wavelength region. It can be seen that the profiles of the diffuse reflectance spectra of pure LCZV host and LCZV:0.01Sm^{3+} phosphors were basically the same. In the NUV range within the wavelength of 200–400 nm, all samples showed an intense absorption band which may be primarily attributed to the ligand to metal CT between V^{5+}–O^{2-} in the VO_4^{3-} tetrahedral group.[36–38] Specially, a small sharp absorption peak at 404 nm, which was assigned to the $^6H_{5/2} \rightarrow {}^4F_{7/2}$ transition of Sm^{3+} ions, was observed in the LCZV:0.01Sm^{3+} sample.[39,40] As we know, there is a relation between the absorption coefficient (α) and the optical band gap (E_g) of the prepared compounds, which can be expressed as:[41]

$$\alpha h\nu = A(h\nu - E_g)^n, \quad (1)$$

where the above parameters, such as A and $h\nu$ stand for coefficient and phonon energy, respectively; and the value of n equals to 1/2, 2, 3/2 and 3 is related to the direct, allowed indirect,

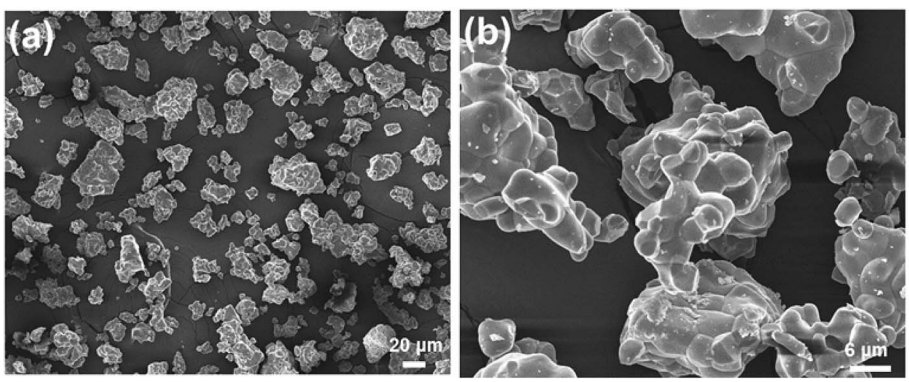

Fig. 2 (a) Low-magnification and (b) high-magnification FE-SEM images of LCZV:0.01Sm^{3+} compounds.

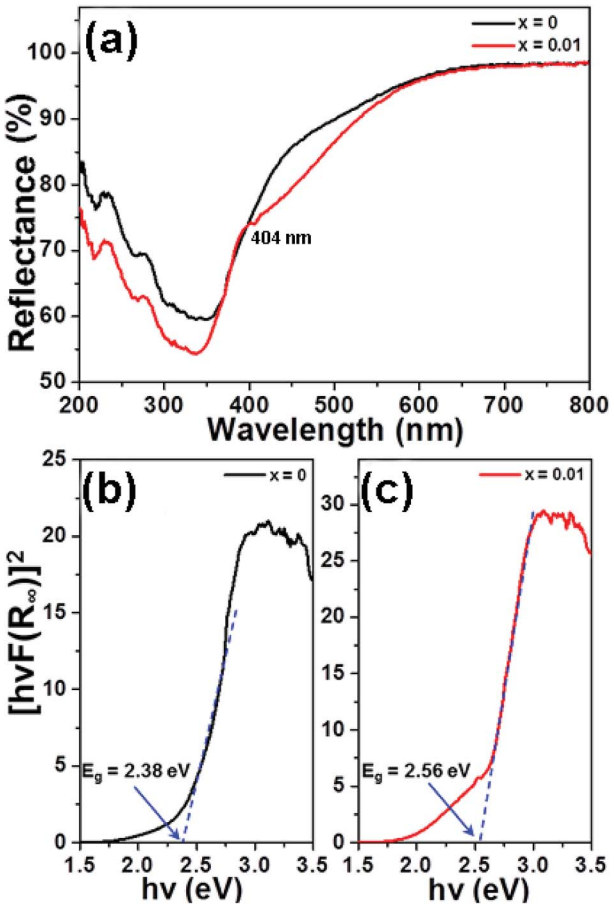

Fig. 3 (a) Diffuse reflectance spectra of the LCZV:xSm^{3+} (x = 0 and 0.01) samples. Calculation of band gap of the (b) LCZV and (c) LCZV:0.01Sm^{3+} phosphors utilizing Kubelka–Munk function.

forbidden direct and forbidden indirect electron transition, respectively. Besides, the absorption spectrum ($F(R_\infty)$) can be achieved from the diffuse reflectance spectrum with the help of following expression:[42]

$$F(R_\infty) = \frac{(1-R)^2}{2R} = \frac{k}{s}, \quad (2)$$

In this formula, R denotes the reflection constant, k shows the molar absorption coefficient and s is attributed to the scattering constant. Thus, by means of the aforementioned equations, the following formula was deduced:[43]

$$[h\nu F(R_\infty)]^{1/n} = B(h\nu - E_g), \quad (3)$$

where B represents the coefficient. As a consequence, when the value of $[h\nu F(R_\infty)]^{1/n}$ is 0, the optical phonon energy of the synthesized samples can be obtained. From Fig. 3(b) and (c), it can be seen that the fitting results were the best when $n = 1/2$. Additionally, the E_g values of LCZV and LCZV:0.01Sm^{3+} compounds were 2.38 and 2.56 eV, respectively. Clearly, with the introduction of Sm^{3+} ions, the optical phonon energy was enhanced, which can be assigned to the Burstein–Moss effect.[44,45] On the basis of the Burstein–Moss effect, one obtains that the enhanced optical band gap of ΔE_g can be expressed as:

$$\Delta E_g = \left(\frac{h}{4\pi m^*_{eh}}\right)(3\pi^2 n)^{2/3}, \text{ and } \frac{1}{m^*_{eh}} = \frac{1}{m^*_e} + \frac{1}{m^*_h}, \quad (4)$$

In this expression, the involved parameters of h, n, m^*_e and m^*_h are associated with Planck constant, carrier concentration, effective masses of electron and hole, respectively. As a consequence, with the addition of Sm^{3+} ions into the LCZV host lattices, the carrier concentration will be increased, leading to the broaden optical band gap in the studied samples.

The intrinsic luminescent behaviors of the selected LCZV host were characterized by the PLE and PL spectra. Fig. 4(a) shows the PLE (λ_{em} = 500 nm) and PL (λ_{ex} = 343 nm) spectra of the LCZV host. As presented, the PLE spectrum consisted of a broad absorption in the wavelength range of 200–400 nm and it can be decomposed into two peaks with the shoulders at around 309 and 343 nm due to the $^1A_1 \rightarrow {}^1T_2$ and $^1A_1 \rightarrow {}^1T_1$ transitions of VO_4^{3-} group, respectively.[46] The LCZV host can emit blue-green emission at the excitation of 343 nm. The PL emission spectrum consists of a broadband with a central wavelength of about 500 nm (Fig. 4(a)). Notably, the broad emission band can also be decomposed into two Gaussian emission bands at approximately 496 nm ($^3T_2 \rightarrow {}^1A_1$ transition) and 605 nm ($^3T_1 \rightarrow {}^1A_1$ transition).[47] The simplified energy level diagram of the VO_4^{3-} group was molded and depicted in Fig. 4(b) to illustrate the UV light-induced visible emissions in the LCZV host.

The luminescence characteristics of the typical LCZV:0.01Sm^{3+} phosphors were also investigated and the results are shown in Fig. 4(c). The detected PLE spectrum monitored at 651 nm exhibited a broad absorption band and several sharp peaks. Particularly, the intense absorption band was assigned to the absorption of VO_4^{3-} groups, whereas the other narrow peaks were associated with the 4f–4f transitions of Sm^{3+} ions from $^6H_{5/2}$ to $^4F_{7/2}$ (404 nm), $(^6P, {}^4P)_{5/2}$ (413 nm), $^4G_{9/2}$ (453 nm) and $^4I_{11/2}$ (465 nm).[48] Since the excitation band at 343 nm showed the strongest intensity in comparison with other peaks, the 343 nm light was thus selected as the excitation light source. As described in Fig. 4(c), the PL spectrum, which was recorded under 343 nm excitation, exhibited several emission peaks at 573, 623, 651 and 708 nm arising from the intra-4f orbital transitions of Sm^{3+} ions from $^4G_{5/2}$ to ^6H_J (J = 5/2, 7/2, 9/2, and 11/2), respectively.[49] Apart from these narrow emission peaks, a broad emission band, which was assigned to the VO_4^{3-} groups, was also observed. These results revealed that the excitation energy can be transferred from the VO_4^{3-} groups to the Sm^{3+} ions. The simplified energy level diagram of VO_4^{3-} groups and Sm^{3+} ions were applied to elaborate the involved luminescence process as well as the involved energy transfer process, as illustrated in Fig. 4(d).

It has been widely accepted that the performance of the rare-earth ion activated luminescent materials can be significantly affected by the dopant concentration. In order to find out the optimal doping concentration of Sm^{3+} ions in the LCZV host, a series of LCZV:xSm^{3+} phosphors were synthesized. Fig. 5(a) shows the PL spectra of LCZV:xSm^{3+} (x = 0, 0.002, 0.005, 0.01, 0.02, 0.03, and 0.04) phosphors, which was excited at 343 nm, as a function of different concentrations of Sm^{3+} ions. It can be

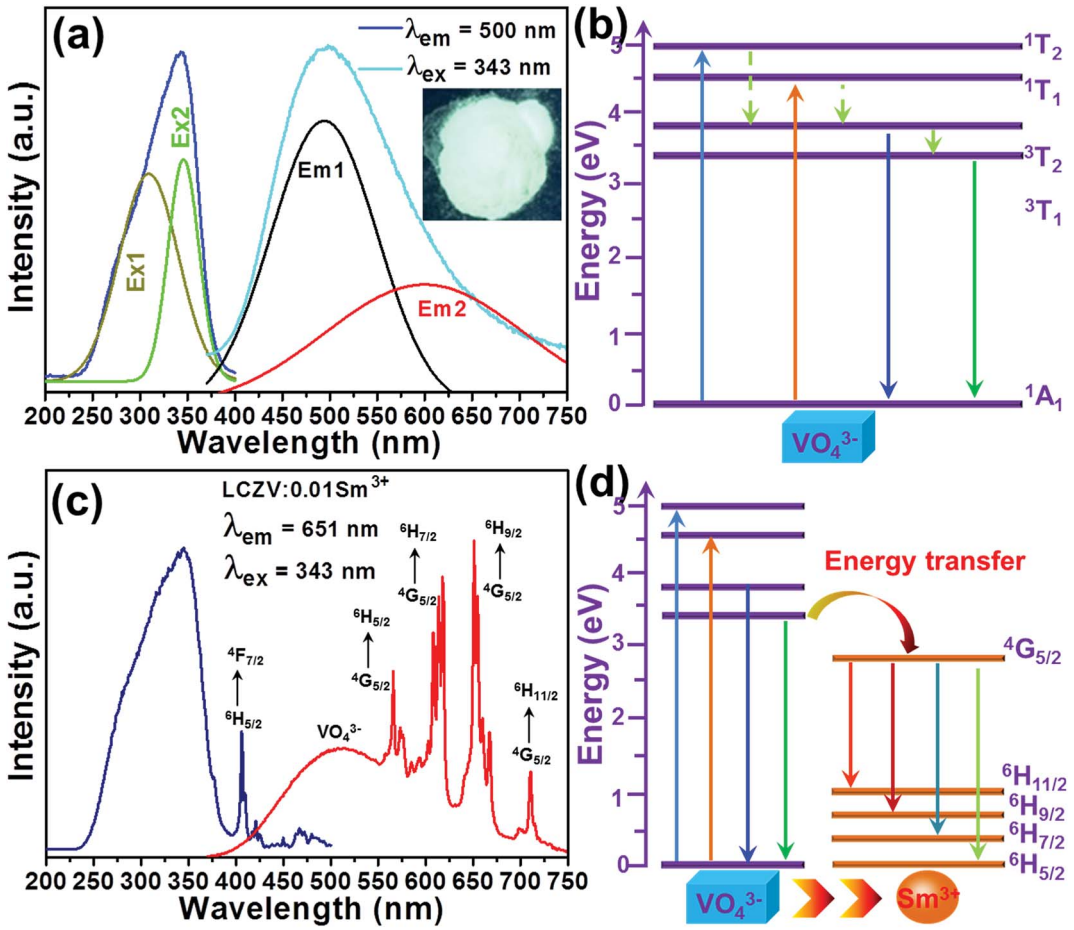

Fig. 4 (a) PLE and PL spectra of LCZV. Inset shows the digital photos of the samples under a 365 nm UV lamp. (b)The excitation and emission processes in VO_4^{3-} tetrahedron with the T_d symmetry in LCZV:xSm^{3+} phosphors. (c) PLE and PL spectra of LCZV:0.01Sm^{3+} phosphors. (d) Schematic diagram of energy transfer process from VO_4^{3-} groups to Sm^{3+} ions.

seen from Fig. 5(a) that all the samples had similar emission profiles and the PL emission intensity was greatly influenced by the dopant content. As demonstrated in Fig. 5(b), the PL emission intensity of the VO_4^{3-} group declined monotonously with the increment of Sm^{3+} ions, whereas that of the Sm^{3+} ions had diverse change tendency (see Fig. 5(c)). With elevating the dopant concentration, the PL emission intensity of the Sm^{3+} ions initially increased, achieving its optimal value when $x = 0.01$, and then, the concentration quenching effect took place when $x > 0.01$. The inconsistent variation tendencies between the PL emission intensities of the VO_4^{3-} group and Sm^{3+} ions further implied the existence of energy transfer from VO_4^{3-} group to Sm^{3+} ions in the LCZV:xSm^{3+} compounds.

To get deeper insight into the involved energy transfer between the VO_4^{3-} group and Sm^{3+} ions, the energy transfer efficiency should be analyzed. According to previous literatures, the energy transfer efficiency between the sensitizer and activator can be roughly estimated from the PL emission spectra by utilizing the following expression:[50]

$$\eta = 1 - \frac{I_S}{I_{S_0}}, \quad (5)$$

where the parameters of η, I_S and I_{S_0} denote the energy transfer efficiency, integrated PL emission intensities of VO_4^{3-} groups with the presence and absence of dopant, respectively. According to eqn (5) and the measured PL emission spectra (Fig. 5(a)), the energy transfer efficiency as a function of Sm^{3+} ion concentration was evaluated and the corresponding results were demonstrated in Fig. 5(d). Obviously, the estimated energy transfer efficiency was dependent on the dopant concentration and its maximum value was decided to be as high as 58.4% when $x = 0.04$. These results suggested that the energy transfer from VO_4^{3-} groups to Sm^{3+} ions in the LCZV:xSm^{3+} phosphors was efficient.

3.3 Colorific properties and quantum efficiency of the resultant phosphors

For the sake of understanding the multicolor emission properties of the as-synthesized compounds, their colorific behaviors were studied. Based on the detected PL emission spectra, the Commission Internationale de l'Eclairage (CIE) coordinates of the LCZV:xSm^{3+} phosphors as a function of Sm^{3+} concentrations were calculated. As shown in Fig. 6(a), the emitting color of the studied samples was verified from bluish-green to

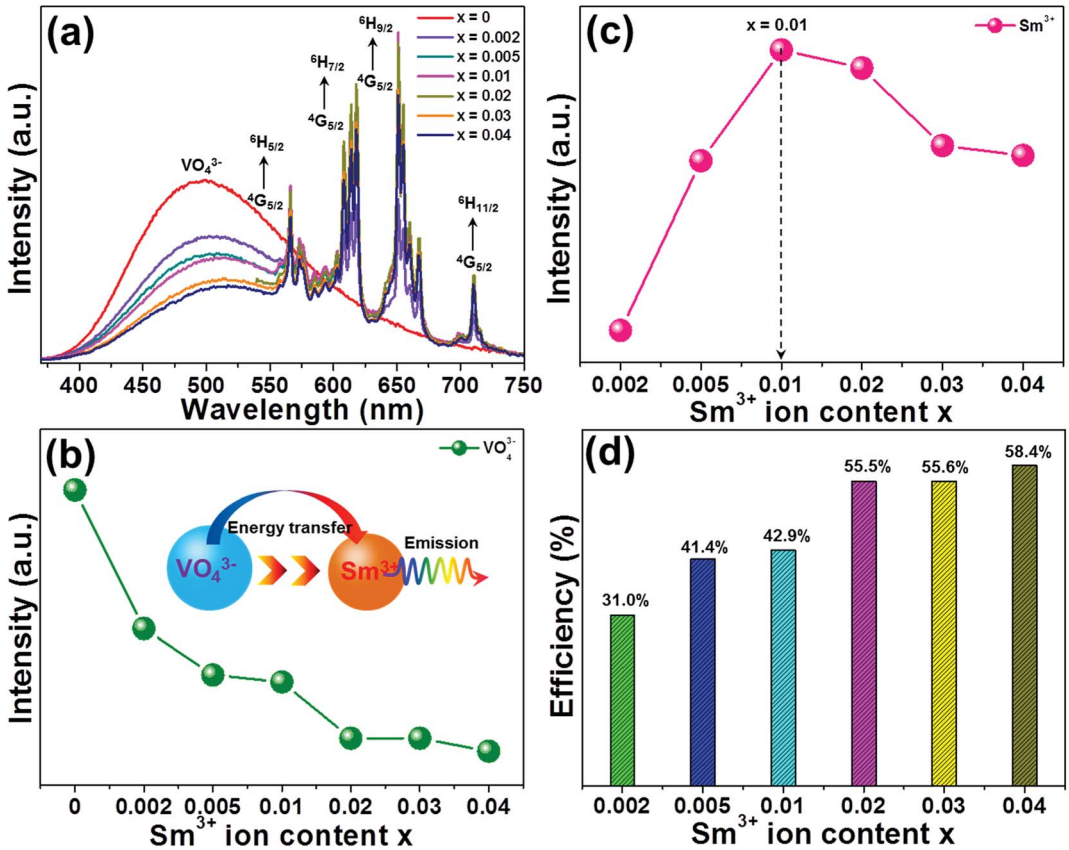

Fig. 5 (a) PL spectra of LCZV:xSm^{3+} phosphors under 343 nm excitation. Dependences of PL emission intensities of (b) VO_4^{3-} groups and (c) Sm^{3+} ions on Sm^{3+} doping concentrations. (d) Energy transfer efficiency from VO_4^{3-} groups to Sm^{3+} ions as a function of Sm^{3+} ion concentration.

white with the addition of Sm^{3+} ion concentration. Meanwhile, the color coordinates of the LCZV:xSm^{3+} compounds were also changed from (0.265, 0.361) to (0.397, 0.395), as listed in Table S3.† These results confirmed that color-tunable emissions can be obtained in the LCZV:xSm^{3+} phosphors. The CCT values of the visible emissions for LCZV:xSm^{3+} phosphors can be calculated by using the McCamy's empirical formula, as described follows below:[51]

$$\mathrm{CCT} = -449n^3 + 3525n^2 - 6823n + 5520.33, \quad (6)$$

where $n = (x - x_e)/(y - y_e)$ is the inverse slope of the line; while $x_e = 0.332$ and $y_e = 0.186$ are the coordinates of the epicentre. The CCT values of LCZV:xSm^{3+} phosphors calculated from eqn (6) were listed in Table S3.† It was noticed that the CCT values varied from 8690 to 3684 K with the increase of Sm^{3+} ion concentration. These obtained characteristics revealed that the Sm^{3+}-doped LCZV phosphors with multicolor emissions and proper CCT values may have potential application in solid-state lighting.

To further verify the suitability of the as-synthesized phosphors for indoor illumination, the IQE of LCZV:xSm^{3+} phosphors should be investigated apart from the above the colorific properties. Fig. 6(b) shows the PLE and PL spectra of the LCZV:0.01Sm^{3+} phosphors and $BaSO_4$ reference sample so as to estimate the IQE of LCZV:0.01Sm^{3+} phosphors. The value of IQE (η_{int}) can be calculated by the following formula:[52]

$$\eta_{int} = \frac{E_i(\lambda) - (1 - A)E_0(\lambda)}{L_e(\lambda)A} \quad (7)$$

where $E_i(\lambda)$ is the integrated luminescence upon direct excitation and $E_0(\lambda)$ is the integrated luminescence excited by indirect illumination from the integrated sphere. The term $L_e(\lambda)$ is the integrated excitation profile obtained from the empty integrated sphere (in the absence of sample). The optical absorbance A can be calculated by using the eqn:

$$A = \frac{L_0(\lambda) - L_i(\lambda)}{L_0(\lambda)} \quad (8)$$

where $L_0(\lambda)$ is the integrated excitation profile when the sample is diffusely illuminated by the surface of the integrated sphere and $L_i(\lambda)$ is the integrated excitation profile when the sample is directly excited by the incident beam.[53] Based on the luminescence spectra, the IQE of LCZV:0.01Sm^{3+} phosphors was calculated to be about 36.1%.

3.4 EL properties of the developed WLEDs device

In order to verify the practicability of the resultant phosphors for the indoor illumination, a white LED device was constructed

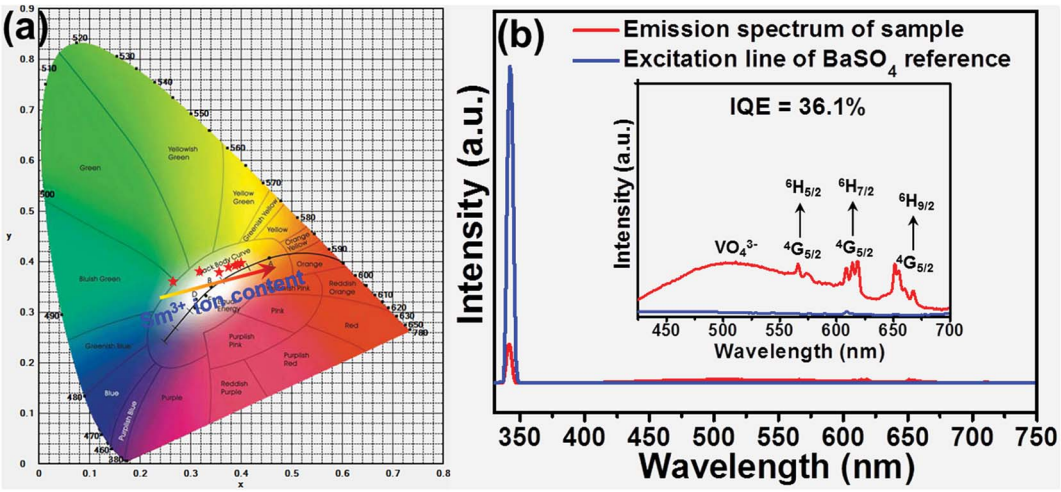

Fig. 6 (a) CIE chromaticity diagram for LCZV:xSm^{3+} phosphors as a function of Sm^{3+} ion concentration. (b) The measurement of IQE of typical LCZV:0.01Sm^{3+} phosphors.

by coating the LCZV:0.01Sm^{3+} phosphors and commercial BAM:Eu^{2+} blue-emitting phosphors onto a commercial NUV LED chip with central wavelength around 365 nm. Under a forward basis current of 100 mA, the electroluminescence (EL) spectrum of the packaged LED device was detected and shown in Fig. 7(a). As presented, the sharp band located in the NUV region was associated to the emission of the NUV LED chip and the broad band centered at around 460 nm was attributed to the emission of the commercial BAM:Eu^{2+} blue-emitting phosphors, while residual emission peaks ranging from 483 to 720 nm were assigned to the emissions of the LCZV:0.01Sm^{3+} phosphors. Fig. 7(b) depicts the packaged white LED device. Clearly, when the injection current was 100 mA, the fabricated LED device can emit dazzling visible white light. Furthermore, the values of CIE coordinates, CRI and CCT were found to be (0.374, 0.398), 88.4, and 4320 K, respectively, when the forward basis current was 100 mA, as displayed in the inset of Fig. 7(a). These observed results revealed that the Sm^{3+}-doped LCZV phosphors were suitable for indoor illumination.

3.5 Temperature sensing properties of Sm^{3+}-doped LCZV phosphors

The temperature-dependent PL emission spectra of the typical LCZV:0.01Sm^{3+} phosphors were measured in order to investigate the optical thermometric behaviors of the studied samples. From the temperature-dependent PL emission spectra (see Fig. 8(a)), one knows that the PL emission intensities exhibited a downward tendency with the increase of temperature owing to the thermal quenching effect. Note that, with rising the

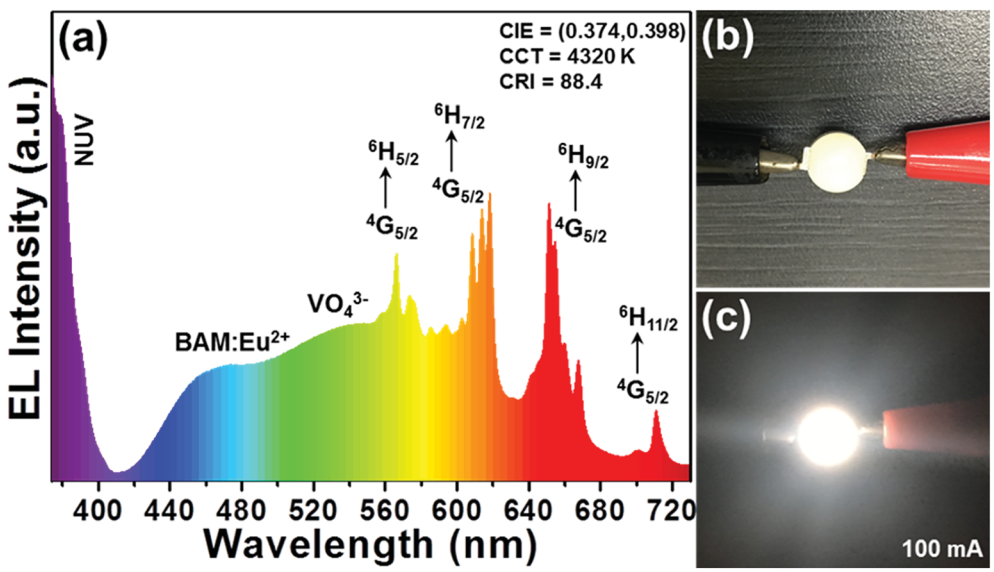

Fig. 7 (a) EL spectrum of the fabricated white LED device recorded at 100 mA. (b) The fabricated white LED device and (c) luminescent image of the white LED device under 100 mA driven current.

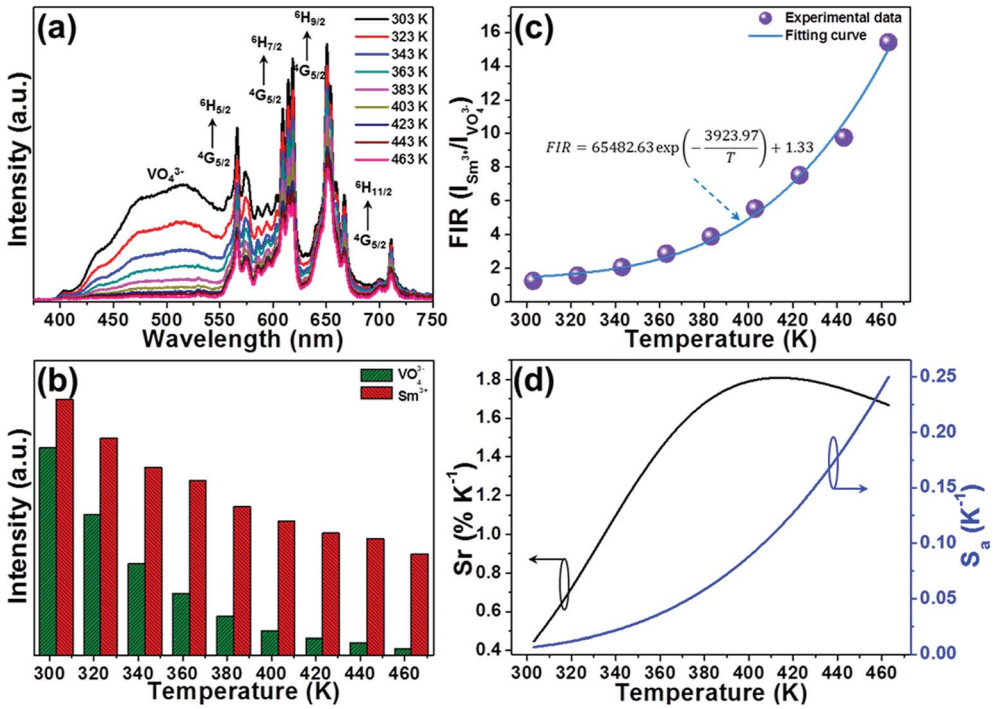

Fig. 8 (a) Temperature-dependent PL emission spectra of LCZV:0.01Sm^{3+} phosphors. (b) PL emission intensities of VO_4^{3-} groups and Sm^{3+} ions as a function of temperature. (c) Plot of FIR *vs.* temperature. (d) Temperature-dependent S_r and S_a for the of LCZV:0.01Sm^{3+} phosphors.

temperature from 303 to 463 K, the PL emission intensity of the VO_4^{3-} groups declined sharply, while that of the Sm^{3+} ions slowly declined, as demonstrated in Fig. 8(b). According to Struck and Fonger's report, it is clear that the relation between the PL emission intensity and temperature can be expressed as:[54]

$$I = \frac{I_0}{1 + A\exp(-\Delta E/kT)}, \tag{9}$$

where I_0 and I are assigned to the PL emission intensities at initial temperature and monitored temperature T, respectively, A is coefficient, ΔE refers to the activation energy and k stands for the Boltzmann constant. As disclosed in Fig. S2,† the detected temperature-dependent PL emission intensities of VO_4^{3-} groups and Sm^{3+} ions can be well fitted by eqn (9). Since the PL emission intensities of the VO_4^{3-} groups and Sm^{3+} ions exhibited diverse responses to the temperature, the FIR value of Sm^{3+} ions to VO_4^{3-} groups would be greatly affected by the temperature which makes the Sm^{3+}-doped LCZV compounds have potential applications for non-contact optical temperature sensors. The temperature-dependent FIR value, which was evaluated from the detected PL emission spectra, was illustrated in Fig. 8(c). As disclosed, the obtained FIR value increased sharply with elevating the temperature from 303 to 463 K. On the other hand, with the aid of eqn (9), the FIR value of Sm^{3+} ions to VO_4^{3-} groups in the LCZV:Sm^{3+} system can be deduced, as defined below:[28]

$$\begin{aligned}\mathrm{FIR} &= \frac{I_{Sm^{3+}}}{I_{VO_4^{3-}}} \\ &= \frac{I_{0,Sm^{3+}}}{I_{0,VO_4^{3-}}} \frac{1 + A_{VO_4^{3-}}\exp\left(-\Delta E_{VO_4^{3-}}/kT\right)}{1 + A_{Sm^{3+}}\exp(-\Delta E_{Sm^{3+}}/kT)} \approx B \\ &\quad + C\exp(-E/kT),\end{aligned} \tag{10}$$

In this expression, B, C and E are parameters which are associated to the I_0, A and ΔE of Sm^{3+} ions and VO_4^{3-} groups. Obviously, the estimated FIR values can be well fitted by eqn (10) (see Fig. 8(c)). Additionally, as disclosed in previous literatures, one knows that the products temperature from the experimental observation for each FIR value can be estimated with the aid of following expression:[55]

$$T = \frac{1}{\ln C - \ln(\mathrm{FIR} - B)} \times \frac{E}{k}, \tag{11}$$

Here, the values of B, C and E/k were 1.33, 65482.63, and 3923.97, respectively. As a consequence, the average difference between the theoretical and observed temperatures was around ±2.25 K.

To get deeper insight into the temperature sensitising properties of the studied samples, their sensor sensitivities should be analyzed. Based on the previous literatures, the absolute sensor sensitivity (S_a) and relative sensor sensitivity (S_r) can be evaluated by utilizing the following expressions:

$$S_a = \frac{\mathrm{d(FIR)}}{\mathrm{d}T} = C\exp\left(\frac{-E}{kT}\right)\left(\frac{E}{kT^2}\right), \tag{12}$$

Table 1 Temperature sensing range, excitation wavelength, maximum S_a and S_r of RE ions-based optical thermometers

Compounds	Temperature	λ_{ex}	S_r	S_a	Reference
$Na_5Gd_9F_{32}:Er^{3+}$	300–510 K	980 nm	1.11%	0.0018 K^{-1}	56
$NaYF_4:Ce^{3+}/Tb^{3+}/Eu^{3+}$	303–563 K	248 nm	1.17%	0.012 K^{-1}	57
$LaOBr:Ce^{3+}/Tb^{3+}$	273–493 K	350 nm	—	0.014 K^{-1}	30
$NaYb_2F_7:Er^{3+}$	300–773 K	980 nm	1.36%	0.0032 K^{-1}	58
$Gd_2(MoO_4)_3:Er^{3+}/Yb^{3+}/Au$	312–723 K	980 nm	—	0.024 K^{-1}	59
$BiF_3:Er^{3+}/Yb^{3+}$	291–691 K	980 nm	1.51%	0.0065 K^{-1}	60
$Ba_5Gd_8Zn_4O_{21}:Yb^{3+}/Tm^{3+}$	300–510 K	980 nm	—	0.0061 K^{-1}	61
$LCZV:xSm^{3+}$	303–463 K	352 nm	1.81%	0.25 K^{-1}	This work

$$S_r = 100\% \times \frac{1}{FIR}\frac{d(FIR)}{dT} = 100\% \times \frac{C\exp(E/kT)}{B + C\exp(-E/kT)} \times \frac{E}{kT^2}, \quad (13)$$

In these expressions, the parameters including, B, C, k, E and T possessed the same meaning as demonstrated in eqn (10). By means of above equations as well as the fitted results displayed in Fig. 8(c), the S_a and S_r values for the LCZV:0.01Sm^{3+} phosphors as a function of temperature were calculated, as presented in Fig. 8(d). It was obvious that the S_a value showed a monotonously increasing tendency with the increment of temperature and reached its maximum value of around 0.25 K^{-1} at 463 K, whereas the S_r value possessed a different changed tendency. As demonstrated in Fig. 8(d), the S_r value firstly increased with the temperature, achieving its optimal value of 1.81% when the temperature was 412 K, and started to decrease with further arising the temperature. In comparison with other reported inorganic optical thermometric materials, as listed in Table 1, the resultant compounds exhibited superior temperature sensing properties with high S_a and S_r values, implying that the Sm^{3+}-doped LCZV phosphors were promising candidates for non-invasion optical thermometry by using the FIR route.

3.6 Temperature-dependent colorific behaviors

As demonstrated above, the PL emission intensities of VO_4^{3-} groups and Sm^{3+} ions exhibited various responses to the temperature (see Fig. 8(a)). Specially, the PL emission intensity of the VO_4^{3-} groups showed a faster decreasing tendency than that of the Sm^{3+} ions, making the emitting color of the studied compounds strongly dependent on the temperature. As a proof of concept, the color coordinates of the typical LCZV:0.01Sm^{3+} phosphors at different temperature were calculated and shown in Fig. 9. Clearly, with arising the temperature from 303 to 463 K, the CIE coordinates were changed from (0.364, 0.388) to (0.569, 0.391), and the emitting color of the studied samples was tuned from white to yellow and finally to red (see inset of Fig. 9).

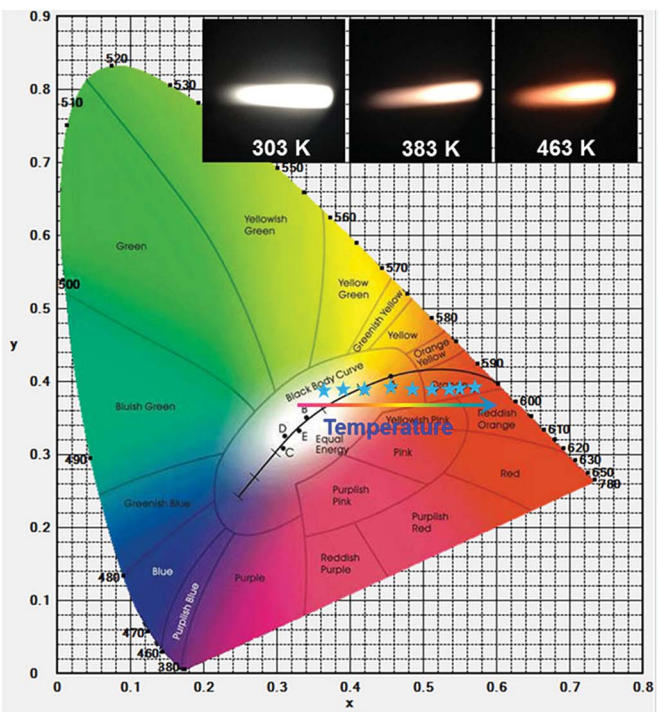

T	x	y
303 K	0.364	0.388
323 K	0.389	0.390
343 K	0.420	0.390
363 K	0.456	0.392
383 K	0.485	0.389
403 K	0.515	0.389
423 K	0.535	0.389
443 K	0.550	0.389
463 K	0.569	0.391

Fig. 9 CIE chromaticity diagram of the LCZV:0.01Sm^{3+} phosphors as a function of temperature. Inset shows the luminescent images excited by 343 nm light.

This temperature-dependent emitting color behavior in the Sm^{3+}-doped LCZV phosphors indicated that the resultant compounds also had potential application in high-temperature environment as safety signal.

4. Conclusion

A series of novel LCZV:xSm^{3+} multicolor-emitting phosphors were successfully synthesized by the solid-state reaction method. Upon 343 nm UV light excitation, the LCZV host emitted bluish-green light from the VO_4^{3-} groups. With the introduction of Sm^{3+} ions into the LCZV host, color controllable emissions were observed in the resultant compounds and the optimal doping concentration was found to be 1 mol%. Moreover, the IQE of the LCZV:0.01Sm^{3+} phosphors was measured to be about 36.1%. With the help of the as-prepared LCZV:0.01Sm^{3+} phosphors, commercial BAM:Eu^{2+} blue-emitting phosphors and a 365 nm NUV-emitting LED chip, a white LED device was prepared. At a 100 mA forward current the obtained white LED can emit bright white light with good CIE coordinates, CRI and CCT values of (0.374, 0.398), 88.4 and 4320 K, respectively. According to the thermal quenching behaviors of the VO_4^{3-} groups and Sm^{3+} ions, the temperature sensing behaviors of the Sm^{3+}-doped LCZV phosphors were studied. It was found that the maximum S_r and S_a values for the LCZV:0.01Sm^{3+} phosphors reached up to 1.81% K^{-1} ($T = 412$ K) and 0.25 K^{-1} ($T = 463$ K), respectively. Furthermore, with arising the temperature from 303 to 463 K, the CIE coordinates were changed from (0.364, 0.388) to (0.569, 0.391), and the emitting color of the studied samples was tuned from white to yellow and finally to red. The obtained results indicated that the Sm^{3+}-doped LCZV phosphors were promising multifunctional materials for simultaneous indoor illumination, non-contact optical thermometer and safety signal in high temperature environment.

Conflicts of interest

There are no conflicts to declare.

Acknowledgements

This work was supported by the National Natural Science Foundation of China (No. 51502190), the Program for the Outstanding Innovative Teams of Higher Learning Institutions of Shanxi, and the Open Fund of the State Key Laboratory of Luminescent Materials and Devices (South China University of Technology, No. 2017-skllmd-01).

References

1 X. Huang, B. Li, H. Guo and D. Chen, *Dyes Pigm.*, 2017, **143**, 86–94.
2 R. Cao, D. Peng, H. Xu, Z. Luo, H. Ao, S. Guo and J. Fu, *Optik*, 2016, **127**, 7896–7901.
3 J. Huang, Q. Li and D. Chen, *Mater. Sci. Eng., B*, 2010, **172**, 108–113.
4 Y. Li, X. Wei, H. Chen, G. Pang, Y. Pan, L. Gong, L. Zhu, G. Zhu and Y. Ji, *J. Lumin.*, 2015, **168**, 124–129.
5 X. Huang, *J. Alloys Compd.*, 2017, **690**, 356–359.
6 X. Huang, H. Guo and B. Li, *J. Alloys Compd.*, 2017, **720**, 29–38.
7 H. Guo, X. Huang and Y. Zeng, *J. Alloys Compd.*, 2018, **741**, 300–306.
8 X. Huang, S. Wang, B. Li, Q. Sun and H. Guo, *Opt. Lett.*, 2018, **43**, 1307–1310.
9 J. Li, K. Qiu, J. Li, W. Li, Q. Yang and J. Li, *Mater. Res. Bull.*, 2010, **45**, 598–602.
10 W.-Q. Yang, H.-G. Liu, M. Gao, Y. Bai, J.-T. Zhao, X.-D. Xu, B. Wu, W.-C. Zheng, G.-K. Liu and Y. Lin, *Acta Mater.*, 2013, **61**, 5096–5104.
11 F. Chen and X. Liu, *Opt. Mater.*, 2013, **35**, 2716–2720.
12 R. Cao, T. Fu, Y. Cao, H. Ao, S. Guo and G. Zheng, *Mater. Lett.*, 2015, **155**, 68–70.
13 X. Zhang, J. Song, L. Zhou, P. He and M. Gong, *Int. J. Appl. Ceram. Technol.*, 2015, **12**, 738–744.
14 X. Dong, J. Zhang, X. Zhang, Z. Hao and Y. Luo, *J. Alloys Compd.*, 2014, **587**, 493–496.
15 H. Guo, B. Devakumar, B. Li and X. Huang, *Dyes Pigm.*, 2018, **151**, 81–88.
16 J. Liang, P. Du, H. Guo, L. Sun, B. Li and X. Huang, *Dyes Pigm.*, 2018, **157**, 40–46.
17 A. R. Dhobale, M. Mohapatra, V. Natarajan and S. V. Godbole, *J. Lumin.*, 2012, **132**, 293–298.
18 L. Wang, H. M. Noh, B. K. Moon, B. C. Choi, J. H. Jeong and J. Shi, *J. Alloys Compd.*, 2016, **663**, 808–817.
19 S. K. Hussain, T. T. H. Giang and J. S. Yu, *J. Alloys Compd.*, 2018, **739**, 218–226.
20 Q. Min, W. Bian, Y. Qi, W. Lu, X. Yu, X. Xu, D. Zhou and J. Qiu, *J. Alloys Compd.*, 2017, **728**, 1037–1042.
21 Y. Gao, F. Huang, H. Lin, J. Zhou, J. Xu and Y. Wang, *Adv. Funct. Mater.*, 2016, **26**, 3139–3145.
22 H. Suo, X. Zhao, Z. Zhang, T. Li, E. M. Goldys and C. Guo, *Chem. Eng. J.*, 2017, **313**, 65–73.
23 X. Wang, Q. Liu, Y. Bu, C.-S. Liu, T. Liu and X. Yan, *RSC Adv.*, 2015, **5**, 86219–86236.
24 P. Du and J. S. Yu, *Chem. Eng. J.*, 2017, **327**, 109–119.
25 Z. Liang, F. Qin, Y. Zheng, Z. Zhang and W. Cao, *Sens. Actuators, A*, 2016, **238**, 215–219.
26 H. Lu, H. Hao, Y. Gao, D. Li, G. Shi, Y. Song, Y. Wang and X. Zhang, *Microchim. Acta*, 2017, **184**, 641–646.
27 L. Marciniak, A. Pilch, S. Arabasz, D. Jin and A. Bednarkiewicz, *Nanoscale*, 2017, **9**, 8288–8297.
28 F. Huang and D. Chen, *J. Mater. Chem. C*, 2017, **5**, 5176–5182.
29 D. Chen, S. Liu, Z. Wan and Z. Ji, *J. Phys. Chem. C*, 2016, **120**, 21858–21865.
30 X. Zhang, Y. Huang and M. Gong, *Chem. Eng. J.*, 2017, **307**, 291–299.
31 D. Chen, S. Liu, W. Xu and X. Li, *J. Mater. Chem. C*, 2017, **5**, 11769–11780.
32 L. Fang, C. Su, H. Zhou, Z. Wei, H. Zhang and N. Alford, *J. Am. Ceram. Soc.*, 2013, **96**, 688–690.
33 P. Dang, S. Liang, G. Li, Y. Wei, Z. Cheng, H. Lian, M. Shang, A. A. Al Kheraif and J. Lin, *Inorg. Chem.*, 2018, **57**, 9251–9259.

34 P. Du and J. S. Yu, *Dyes Pigm.*, 2017, **147**, 16–23.
35 T. Hasegawa, Y. Abe, A. Koizumi, T. Ueda, K. Toda and M. Sato, *Inorg. Chem.*, 2018, **57**, 857–866.
36 T. Li, P. Li, Z. Wang, S. Xu, Q. Bai and Z. Yang, *RSC Adv.*, 2015, **5**, 71735–71742.
37 B. V. Rao, K. Jang, H. S. Lee, S.-S. Yi and J.-H. Jeong, *J. Alloys Compd.*, 2010, **496**, 251–255.
38 Z. Tao, T. Tsuboi, Y. Huang, W. Huang, P. Cai and H. J. Seo, *Inorg. Chem.*, 2014, **53**, 4161–4168.
39 F. Yang, Z. Yang, Q. Yu, Y. Liu, X. Li and F. Lu, *Spectrochim. Acta, Part A*, 2013, **105**, 626–631.
40 Y. Lin, Z. Niu, Y. Han, C. Li, W. Zhou, J. Zhang, L. Yu and S. Lian, *J. Alloys Compd.*, 2017, **690**, 267–273.
41 K. Inaba, S. Suzuki, Y. Noguchi, M. Miyayama, K. Toda and M. Sato, *Eur. J. Inorg. Chem.*, 2008, **2008**, 5471–5475.
42 X. Wang, Z. Zhao, Q. Wu, C. Wang, Q. Wang, L. Yanyan and Y. Wang, *J. Mater. Chem. C*, 2016, **4**, 8795–8801.
43 L. Li, Y. Pan, X. Zhou, C. Zhao, Y. Wang, S. Jiang, A. Suchocki and M. G. Brik, *J. Alloys Compd.*, 2016, **685**, 917–926.
44 E. Burstein, *Phys. Rev.*, 1954, **93**, 632–633.
45 A. P. Roth, J. B. Webb and D. F. Williams, *Solid State Commun.*, 1981, **39**, 1269–1271.
46 Z. Zhou, F. Wang, S. Liu, K. Huang, Z. Li, S. Zeng and K. Jiang, *J. Electrochem. Soc.*, 2011, **158**, H1238.
47 Q. Tang, K. Qiu, J. Li, W. Zhang and Y. Zeng, *J. Mater. Sci.: Mater. Electron.*, 2017, **28**, 18686–18696.
48 V. Rao Bandi, B. K. Grandhe, M. Jayasimhadri, K. Jang, H.-S. Lee, S.-S. Yi and J.-H. Jeong, *J. Cryst. Growth*, 2011, **326**, 120–123.
49 K. Li, M. Shang, H. Lian and J. Lin, *J. Mater. Chem. C*, 2016, **4**, 5507–5530.
50 C. Liu, D. Hou, J. Yan, L. Zhou, X. Kuang, H. Liang, Y. Huang, B. Zhang and Y. Tao, *J. Phys. Chem. C*, 2014, **118**, 3220–3229.
51 C. S. Mccamy, *Color Res. Appl.*, 1992, **17**, 142–144.
52 X. Zhang, J. Song, C. Zhou, L. Zhou and M. Gong, *J. Lumin.*, 2014, **149**, 69–74.
53 F. Xie, Z. Dong, D. Wen, J. Yan, J. Shi, J. Shi and M. Wu, *Ceram. Int.*, 2015, **41**, 9610–9614.
54 C. W. Struck and W. H. Fonger, *J. Appl. Phys.*, 1971, **42**, 4515–4516.
55 P. Du, Y. Hua and J. S. Yu, *Chem. Eng. J.*, 2018, **352**, 352–359.
56 X. Li, J. Cao, F. Hu, R. Wei and H. Guo, *RSC Adv.*, 2017, **7**, 35147–35153.
57 M. Ding, M. Xu and D. Chen, *J. Alloys Compd.*, 2017, **713**, 236–247.
58 F. Hu, J. Cao, X. Wei, X. Li, J. Cai, H. Guo, Y. Chen, C.-K. Duan and M. Yin, *J. Mater. Chem. C*, 2016, **4**, 9976–9985.
59 H. Hao, H. Lu, R. Meng, Z. Nie, G. Ao, Y. Song, Y. Wang and X. Zhang, *J. Alloys Compd.*, 2017, **695**, 2065–2071.
60 P. Du and J. S. Yu, *Microchim. Acta*, 2018, **185**, 237.
61 H. Suo, C. Guo, Z. Yang, S. Zhou, C. Duan and M. Yin, *J. Mater. Chem. C*, 2015, **3**, 7379–7385.